

Modeling and Experimental Analysis of Piezoelectric Shakers for High-Frequency Calibration of Accelerometers

Gregory W. Vogl, Kari K. Harper, and Bev Payne

*National Institute of Standards and Technology
100 Bureau Drive, Stop 8220
Gaithersburg, MD, USA 20899-8220*

Abstract. Piezoelectric shakers have been developed and used at the National Institute of Standards and Technology (NIST) for decades for high-frequency calibration of accelerometers. Recently, NIST researchers built new piezoelectric shakers in the hopes of reducing the uncertainties in the calibrations of accelerometers while extending the calibration frequency range beyond 20 kHz. The ability to build and measure piezoelectric shakers invites modeling of these systems in order to improve their design for increased performance, which includes a sinusoidal motion with lower distortion, lower cross-axial motion, and an increased frequency range. In this paper, we present a model of piezoelectric shakers and match it to experimental data. The equations of motion for all masses are solved along with the coupled state equations for the piezoelectric actuator. Finally, additional electrical elements like inductors, capacitors, and resistors are added to the piezoelectric actuator for matching of experimental and theoretical frequency responses.

Keywords: calibration; accelerometers; vibration; piezoelectric actuation; shakers

PACS: 06.20.fb, 06.30.Gv

INTRODUCTION

For decades, piezoelectric shakers have been developed and used at the National Institute of Standards and Technology (NIST) for calibration of accelerometers [1], and recently, NIST researchers built new piezoelectric shakers in the hopes of enabling calibrations with reduced uncertainties and extended frequency ranges beyond 20 kHz [2]. The ability to build and measure piezoelectric shakers invites modeling of these systems in order to better their designs for improved calibration of accelerometers. Sinusoidal motion of the accelerometer under test along a single axis with lower distortion, lower cross-axial motion, and an increased frequency range is desired.

Piezoelectric shakers have many advantages that make them suitable for high-frequency calibration of accelerometers. For example, these shakers are relatively stiff, may be used at high frequencies (usually above 3 kHz), and are easy to keep in optical alignment [3] for interferometry due to almost no equilibrium excursion [4] from their stiff construction. Furthermore, relatively small piezoelectric shakers can provide much higher accelerations compared to those achievable with electrodynamic shakers for frequencies above 5 kHz. In fact, when a piezoelectric-based exciter vibrates in a state of resonance, a large axial acceleration can be produced with little exciting power [4]. Because many of the primary modes are axial for piezoelectric systems, mechanical resonances could be exploited in those cases to produce satisfactory axial motion. Shakers at NIST have been developed with distributed sets of axial resonances to produce flatter frequency responses over wide frequency ranges [1]. On the other hand, for exciters in which air bearings or flexural elements are used, avoiding resonances is preferable because the resonances are usually associated with non-axial motion.

In this paper, we present a model of piezoelectric shakers and match it to experimental data. The piezoelectric actuator is modeled as a compliant element governed by coupled state equations, and the other shaker parts are modeled as either rigid bodies or simple compliant elements. By considering the excited shaker as a system with a modified impedance due to additional electrical elements, we demonstrate that the results from the model agree fairly well with those from impedance and acceleration experiments. Improvements to the model should help to

illustrate how both electrical and mechanical resonances can be tailored to maximize the performance of piezoelectric shakers.

BASIC DESIGN CONSIDERATIONS

Figure 1 shows the simplest configuration for an axisymmetric piezoelectric shaker (also known as a “piezoshaker”), which is composed of a table cylinder of mass m_1 and a base cylinder of mass m_2 that are separated by a piezoelectric material disk. The accelerometer mounts to the top of the table and, when the piezoelectric material is excited by a sinusoidal voltage, the table and accelerometer will vibrate. In order to acquire acceptable motion of the accelerometer, there are certain guidelines that should be followed in the design of piezoshakers, even for the simple configuration in Figure 1.

One design consideration is the relative masses of the table and base. The shaker is assumed to be weakly coupled to its surrounding environment, and consequently, the shaker can be considered to be “floating” for sufficiently high frequencies. Thus, without any external forces, the center of mass of the shaker cannot change with time, no matter what vibrations are induced by internal forces. This is a crucial fact, because it directly affects the goal to maximize the axial (vertical) displacement of the table. For example, if $m_1 = m_2$, then the table and base will displace the same magnitude, but in opposite directions, due to piezoelectric actuation. On the other hand, if $m_1 \ll m_2$, then the table mass will incur the bulk of the displacement while the base remains relatively still. Therefore, the table displacement for $m_1 \ll m_2$ is almost twice that for $m_1 = m_2$, which leads us to desire that the base mass be much greater than the table mass to maximize the achievable accelerations.

However, the cylinders should not be too large. During high-frequency vibrations, the cylinders used for the piezoshakers need to translate in vibration without being excited themselves. No material is perfectly rigid, yet the cylinders should be rigid enough so that internal modes are not excited. These cylinder-specific modes may lead to large and undesirable cross-axial motions of the accelerometer under test. To minimize the excitation of these modes, their resonant frequencies should be much greater than the calibration frequencies; that is, $v/L \gg f$, where v is the speed of sound in the material, L is a characteristic length of the cylinder, and f is the calibration frequency. Therefore, the sound speed should be as large as possible and the cylinder dimensions should be minimized. Alternatively, because $v = f\lambda$ where λ is the wavelength of sound in the material, we find out that $L \ll \lambda$. In other words, the cylinders should be small relative to the wavelength of sound in the cylinders in order to minimize the excitation of their modes.

Materials with relatively large speeds of sound are chosen to help maximize the resonant frequencies of the cylinders. The main figure of merit for sound speed is the specific modulus, which is the ratio of the elastic modulus to the density and is on the order of the square of the speed of sound. Specific moduli of candidate materials are shown in Table 1 [5].

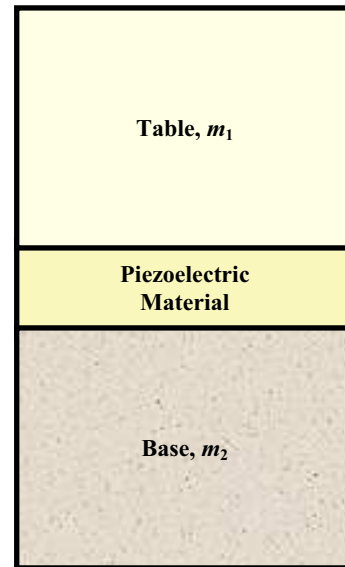


FIGURE 1. Basic Piezoelectric Shaker.

TABLE 1. Candidate Materials for Piezoelectric Shakers

Material	Density, ρ (kg/m^3)	Elastic Modulus, Y (GPa)	Specific Modulus, Y/ρ (km/s^2)
Diamond	3510	1035	295
Beryllium	1850	303	164
Silicon Carbide	3200	390	122
Aluminum Oxide (Alumina)	3900 ^(a)	393	101
Tungsten Carbide	14800 ^(a)	530 ^(b)	36
Titanium	4510	110	24
Piezoelectric Ceramic	7700 ^(c)	54	7

^(a) Approximate measured values for materials at NIST

^(b) Value from Ref. [6]

^(c) Value from manufacturer [7]

Due to the large density difference between alumina and tungsten carbide, alumina was chosen as the material for the table and tungsten carbide was chosen as the material for the base in order to help satisfy $m_1 \ll m_2$. Cost (e.g., for diamond) and safe-handling concerns (e.g., for beryllium) were also factors in material selection.

Finally, not only must the cylinders be small enough, but they must also be wide enough to provide adequate flexural rigidity and resistance to cross-axial rotations. Furthermore, the top surface of the table needs to be sufficiently large to accommodate accelerometers of various sizes as well as reflectors and other calibration aids.

ADVANCED DESIGN CONSIDERATIONS

If all of these criteria are met, then the basic piezoelectric shaker of Fig. 1 should produce an accelerometer frequency response curve with one sharp peak (i.e., a high quality factor) and a resonant frequency that would depend significantly on the accelerometer mass. Beyond the resonant frequency, the shaker would not be very useful for calibrations because the table displacement would become too small.

One way to avoid this problem is by using the method of “stagger tuning” [1] by coupling additional cylinders to the table and base, as seen in Fig. 2. Because of the extra degrees of freedom, additional axial modes exist, which would be seen as additional peaks at various frequencies in the frequency response. These frequencies and mode shapes rely on the connecting material between the masses. Thin disks of polyisobutylene (butyl rubber) connect the extra alumina masses for the shakers in Fig. 2. The butyl rubber disks are seen in the figure as thin black curves.

To a large extent, the resonant frequencies and mode shapes can be “tuned” via adjustments to the thicknesses of the butyl rubber connecting pieces. The main goal is to produce modes that have the largest possible table motions in order to maximize



FIGURE 2. Shakers P102 (Left) and P103 (Right).

the acceleration. Furthermore, the resonant frequencies should be “staggered” or spaced out along a wide frequency domain, with the frequency limit for calibrations being slightly beyond the largest modal frequency. In that case, any frequency for calibration will be “near” a resonance in order to maximize the acceleration.

MODELING OF PIEZOELECTRIC SHAKERS

Shakers P102 and P103 (see Fig. 2) were developed at NIST over the last year [2], but their designs were created at NIST through a trial-and-error process many decades ago [1]. Those designs were revisited recently in order to gain new experience in the assembling and behavior of piezoelectric shakers, with the hopes of extending the frequency range beyond 20 kHz while decreasing the measurement uncertainty. However, in order to accomplish these goals to the fullest, the efficient and modern tools of computer simulations and software should be used to design new piezoshakers before the time-consuming process of assembly begins.

The first step in simulating the motion of the shaker is to create a simplified model that includes the main physics affecting the behavior of the shaker. Figure 3 shows the model used herein for shaker P102. All five masses are labeled as m_1, m_2, \dots, m_5 , and they move axially (vertically) by w_1, w_2, \dots, w_5 from their equilibrium positions as a function of time, t . Because we know *a priori* that the majority of the motion is axial despite some unwanted cross-axial

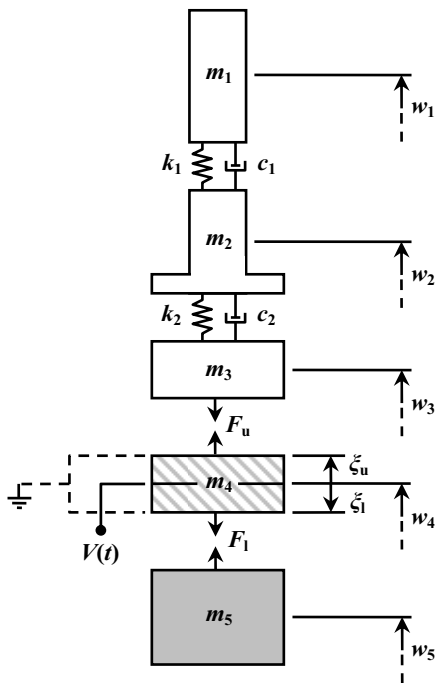


FIGURE 3. Model of Piezoelectric Shaker P102 for Axial Vibrations.

motion, we have assumed that all excitation and displacements are axial. Second, because the cylinder materials were chosen so that cylinder-specific modes are not excited, the alumina and tungsten carbide pieces are modeled as rigid masses. Third, springs and dampers are used to approximate the butyl rubber disks with spring constants k_i and damping coefficients c_i for $i = 1, 2$.

The piezoelectric ceramic actuators are two disks that have been bonded together with conductive epoxy. As seen in Fig. 3, the excitation voltage, V , operates at the interface of the two piezoelectric disks. The remaining upper and lower piezoelectric interfaces are electrically grounded and epoxied to masses m_3 and m_5 , respectively. Hence, the actuators are coupled to the masses via net forces, F_u and F_1 , which are assumed to act via uniform normal stresses at the interfaces. Furthermore, the upper and lower disks have deformed thicknesses of ξ_u and ξ_1 , respectively, which depend on the excitation voltage and the interfacial stresses.

EQUATIONS OF MOTION

The cylinders move according to Newton's second law, which states that the net force on a body equals its mass times the acceleration of its center of mass. Therefore, the governing equations for each of the bodies in Fig. 3 are

$$m_1 \ddot{w}_1 + c_1(\dot{w}_1 - \dot{w}_2) + k_1(w_1 - w_2) = 0 \quad (1a)$$

$$m_2 \ddot{w}_2 + c_2(\dot{w}_2 - \dot{w}_3) + k_2(w_2 - w_3) - c_1(\dot{w}_1 - \dot{w}_2) - k_1(w_1 - w_2) = 0 \quad (1b)$$

$$m_3 \ddot{w}_3 - c_2(\dot{w}_2 - \dot{w}_3) - k_2(w_2 - w_3) = -F_u \quad (1c)$$

$$m_4 \ddot{w}_p = F_u - F_1 \quad (1d)$$

$$m_5 \ddot{w}_5 = F_1 \quad (1e)$$

where w_p is the combined center of mass for the two piezoelectric disks. The variable w_p is not seen in Fig. 3 because Eq. (1d) will not be used, but must still be satisfied for a valid solution. Solution of Eqs. (1) is not yet possible because expressions for the forces F_u and F_1 rely on equations governing the piezoelectric actuation.

Piezoelectric materials can produce electric fields when sensing stresses through the direct piezoelectric effect and, vice versa, can generate large forces and strains through electrical excitation via the inverse piezoelectric effect [8]. The piezoelectric disks used for the NIST piezoshakers are solid, ceramic disks that are axially polarized with the top and bottom flat surfaces fully electroded. The polarization is assumed to be perfectly axial and uniform across the ceramic, so that the excitation is purely axial. Piezoelectric ceramics are categorized as "soft" or "hard" according to whether or not the ceramics contain "donor" or "acceptor" dopants, respectively. Soft ceramics produce large displacements relative to hard ceramics, but they also have greater hysteresis and are more susceptible to depolarization. Hard ceramics, like those used for the shakers in Fig. 2, are able to operate at higher temperatures due to Curie points greater than 300 °C. Even though they cannot produce the same large displacements as soft ceramics, hard ceramics are more stable and compatible with large mechanical loads and voltages [7].

For high precision piezoelectric actuators and sensors, the nonlinear and hysteretic responses under extreme conditions may be detrimental for the performance of the whole device. Up to 70 % of the piezoelectric response is attributed to the activity of non-180° ferroelectric domain walls, and the domain wall contribution has been found out to be the main origin of the instability of the piezoelectric effect [9]. While harmonic distortion is always present, it is known *a priori* that the harmonic distortion is not significant over most of the frequency range.

Consequently, we assume that the piezoelectric actuators operate within a linear regime due to relatively small displacements and voltages. The basic constitutive equations governing the linear behavior of axial strain ε , axial stress σ , electric displacement D , and electric field E in the piezoelectric ceramic for axial excitation and polarity are given in Ref. [10] as

$$\varepsilon = S^E \sigma + d E \quad (2a)$$

$$D = d \sigma + \xi^\sigma E \quad (2b)$$

where the superscripts σ and E denote measurements taken at constant mechanical stress and constant electric field, respectively. In Eq. (2a), S^E is the mechanical compliance for a constant electric field and d is the piezoelectric charge constant. In Eq. (2b), ξ^σ is the dielectric coefficient for a constant stress and the electric displacement D is defined as

$$D = \frac{1}{A} \int I dt \quad (3)$$

where A is the area of the piezoelectric interface and I is the displacement current in the direction of E . We note that Eq. (2b) relies on the assumption that the transduction process is completely reversible [10]. Also, all parameters are assumed to be constant with respect to frequency.

Figure 4 shows a schematic of the piezoelectric ceramic disks. Both disks have an undeformed thickness h and are poled [7] towards each other. In the undeformed state, a coordinate z is set up relative to the interface between the disks. Thus, $z = 0$ to $z = h$ corresponds to the undeformed upper disk and $z = -h$ to $z = 0$ corresponds to the undeformed lower disk. With a voltage V across the disks, every differential element moves with a deformation w as a function of z relative to the initial state, and the upper and lower disk thicknesses change to ζ_u and ζ_l , respectively, as seen in Fig. 3. For simplicity, we designate the direction for deformation w as the same for both disks.

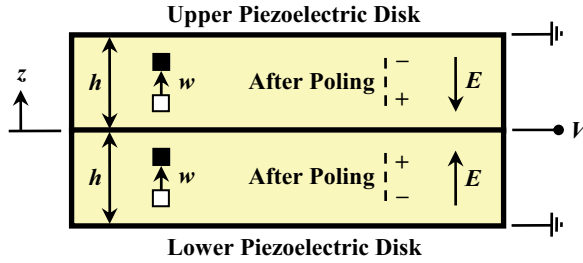


FIGURE 4. Schematic of Piezoelectric Ceramic Disks with Additional Variables and Coordinate System.

With the aid of necessary definitions, Eqs. (2) can be used to derive a different set of governing equations for the piezoelectric material. First, based on Fig. 4, the axial strain ε is defined as

$$\varepsilon = \frac{\partial w}{\partial z} \quad (4)$$

and because the speed of sound is much less than that for light, Poisson's equation applies as

$$E = -\frac{\partial \phi}{\partial z} \quad (5)$$

where ϕ is the electric potential and depends on z [11]. However, within either of the disks, the electric displacement D does not depend on z because the displacement current is constant across the thickness due to conservation of displacement current. Finally, every differential element in the piezoelectric disks must obey Newton's second law, which means that

$$\frac{\partial \sigma}{\partial z} = \rho \ddot{w} \quad (6)$$

where ρ is the density of the piezoelectric disk.

We differentiate Eqs. (2) with respect to z , substitute Eqs. (4)-(6) into the resulting equations, and then solve to find out that

$$\frac{\partial^2 w}{\partial t^2} = v^2 \frac{\partial^2 w}{\partial z^2} \quad (7a)$$

$$\frac{\partial^2 \phi}{\partial z^2} = g \rho v^2 \frac{\partial^2 w}{\partial z^2} \quad (7b)$$

where v is the piezoelectric wave speed, which is defined as

$$v = [\rho(S^E - dg)]^{-1/2} \quad (8)$$

and g is the piezoelectric voltage constant, which is defined as

$$g = \frac{d}{\varepsilon^\sigma} \quad (9)$$

Equation (8) shows how the piezoelectric wave speed is a modified version (note the minus sign in the equation) of the wave speed without any piezoelectric behavior. Also, we stated beforehand that Eq. (1d) will not be used, but

must still be satisfied for a valid solution. Equation (7a) will be used instead of Eq. (1d), and because Eq. (6) (Newton's second law for a differential element) was used in the formulation of Eq. (7a), Newton's second law for the entire piezoelectric body, Eq. (1d), is automatically satisfied.

GENERAL FORM OF SOLUTION

We now formulate the general solution for a sinusoidal voltage $V(t)$ with angular frequency ω and voltage amplitude V_{pk} ; that is,

$$V(t) = V_{pk} \sin(\omega t) \quad (10)$$

Given a sufficient amount of time under this excitation, the piezoelectric shaker will reach an equilibrium vibration with the same frequency. In that case, the general solution of Eq. (7a) is

$$w(z, t) = \sin\left(\frac{\omega z}{v}\right) \left[\bar{A} \sin(\omega t) + \bar{B} \cos(\omega t) \right] + \cos\left(\frac{\omega z}{v}\right) \left[\bar{C} \sin(\omega t) + \bar{D} \cos(\omega t) \right] \quad (11)$$

where variables with bar embellishments are solution parameters yet unknown. However, proper use of Eq. (11) requires one solution, $w_u(z, t)$, for the upper piezoelectric disk and another solution, $w_l(z, t)$, for the lower piezoelectric disk:

$$w(z, t) = \begin{cases} w_u(z, t), & 0 \leq z \leq h \\ w_l(z, t), & -h \leq z \leq 0 \end{cases} \quad (12)$$

where

$$w_u(z, t) = \sin\left(\frac{\omega z}{v}\right) \left[\bar{A}_u \sin(\omega t) + \bar{B}_u \cos(\omega t) \right] + \cos\left(\frac{\omega z}{v}\right) \left[\bar{C}_u \sin(\omega t) + \bar{D}_u \cos(\omega t) \right] \quad (13a)$$

$$w_l(z, t) = \sin\left(\frac{\omega z}{v}\right) \left[\bar{A}_l \sin(\omega t) + \bar{B}_l \cos(\omega t) \right] + \cos\left(\frac{\omega z}{v}\right) \left[\bar{C}_l \sin(\omega t) + \bar{D}_l \cos(\omega t) \right] \quad (13b)$$

Consequently, because of the piecewise-continuous nature of the deformation, the electric displacements are generally different for the two piezoelectric disks. For the given sinusoidal excitation, the electric displacements in the upper and lower disks, respectively D_u and D_l , will reach dynamic equilibrium:

$$D_u(t) = \bar{D}_{u,s} \sin(\omega t) + \bar{D}_{u,c} \cos(\omega t) \quad (14a)$$

$$D_l(t) = \bar{D}_{l,s} \sin(\omega t) + \bar{D}_{l,c} \cos(\omega t) \quad (14b)$$

The rigid bodies in the piezoshaker also reach dynamic equilibrium. Therefore, the solutions of Eqs. (1) are

$$w_i(t) = \bar{A}_i \sin(\omega t) + \bar{B}_i \cos(\omega t) \quad (15)$$

for $i = 1, 2, 3$, or 5 , and the sinusoidal forces F_u and F_l are defined as

$$F_u(t) = \bar{F}_{u,s} \sin(\omega t) + \bar{F}_{u,c} \cos(\omega t) \quad (16a)$$

$$F_l(t) = \bar{F}_{l,s} \sin(\omega t) + \bar{F}_{l,c} \cos(\omega t) \quad (16b)$$

There are a total of 24 solution parameters among Eqs. (12)-(16) that need to be solved for the given voltage in Eq. (10). However, proper boundary conditions are still needed for solution.

BOUNDARY CONDITIONS

The required boundary conditions for solution are related to the piezoelectric deformation. First, because the two piezoelectric disks are bonded together, their displacements must match at the interface, $z = 0$; that is,

$$w_u(0,t) = w_l(0,t) \quad (17)$$

Second, because the upper piezoelectric disk is bonded to the third mass (refer to Fig. 3) and the lower piezoelectric disk is bonded to the fifth mass,

$$w(h,t) = w_3(t) \quad (18a)$$

$$w(-h,t) = w_5(t) \quad (18b)$$

Third, according to Eq. (6), the axial stress σ must be continuous across the interface at $z = 0$ for finite acceleration at the interface. An equation for this condition is found through substitution of Eqs. (2b) and (4) into Eq. (2a) to eliminate the variable E , which yields

$$\frac{\partial w}{\partial z} = (S^E - dg)\sigma + gD \quad (19)$$

Application of Eq. (19) for the upper and lower piezoelectric disks reveals that, for continuity of axial stress σ across the interface at $z = 0$,

$$\left[\frac{\partial w_u}{\partial z} - \frac{\partial w_l}{\partial z} \right]_{z=0} = g(D_u - D_l) \quad (20)$$

Fourth, because Eq. (19) must hold at the upper interface (at $z = h$) where $\sigma = F_u/A$ as well as at the lower interface (at $z = -h$) where $\sigma = F_l/A$, two more boundary conditions are

$$\left[\frac{\partial w}{\partial z} \right]_{z=h} = (S^E - dg) \frac{F_u}{A} + gD_u \quad (21a)$$

$$\left[\frac{\partial w}{\partial z} \right]_{z=-h} = (S^E - dg) \frac{F_l}{A} + gD_l \quad (21b)$$

Fifth, the deformed thicknesses, ξ_u and ξ_l , of the upper and lower disks are related to the electric displacements and applied voltage through the piezoelectric state equations, Eqs. (2). We substitute Eqs. (2b), (4), and (5) into Eq. (2a) to eliminate the variable σ and obtain

$$\frac{\partial w}{\partial z} = \frac{S^E}{d} D + \frac{1}{g} (S^E - dg) \frac{\partial \varphi}{\partial z} \quad (22)$$

Then, we integrate Eq. (22) from $z = 0$ to $z = h$ and also from $z = -h$ to $z = 0$, apply the voltage boundary conditions to the resulting equations, and obtain

$$\xi_u = w(h,t) - w(0,t) = \frac{S^E h}{d} D_u - \frac{1}{g} (S^E - dg) V(t) \quad (23a)$$

$$\xi_l = w(0,t) - w(-h,t) = \frac{S^E h}{d} D_l - \frac{1}{g} (S^E - dg) V(t) \quad (23b)$$

METHOD OF SOLUTION

Equations (17), (18), (20), (21), and (23) total eight (8) boundary conditions. When these are combined with the four (4) equations of motion for the rigid bodies in Eqs. (1), we have a total of twelve (12) equations to be solved. These twelve equations can be used to solve for the twenty-four (24) parameters. By inspection of the general form of the solution, Eqs. (12)-(16), we note that each solution has $\sin(\omega t)$ and $\cos(\omega t)$ terms. When substituted into the twelve equations to be solved, each of the resulting equations will have sine and cosine terms. Equating coefficients of like-terms on both sides of the equations results in twenty-four equations that will not depend on $\sin(\omega t)$ or $\cos(\omega t)$. In other words, the twelve time-dependent equations have doubled to become twenty-four time-independent equations through use of the general solution forms.

Finally, because the twenty-four (24) algebraic equations are linear with respect to the twenty-four (24) solution parameters, there is one unique solution for the non-homogeneous system of equations. These equations can be solved using linear equation solvers in a variety of mathematics software.

EXPERIMENTS

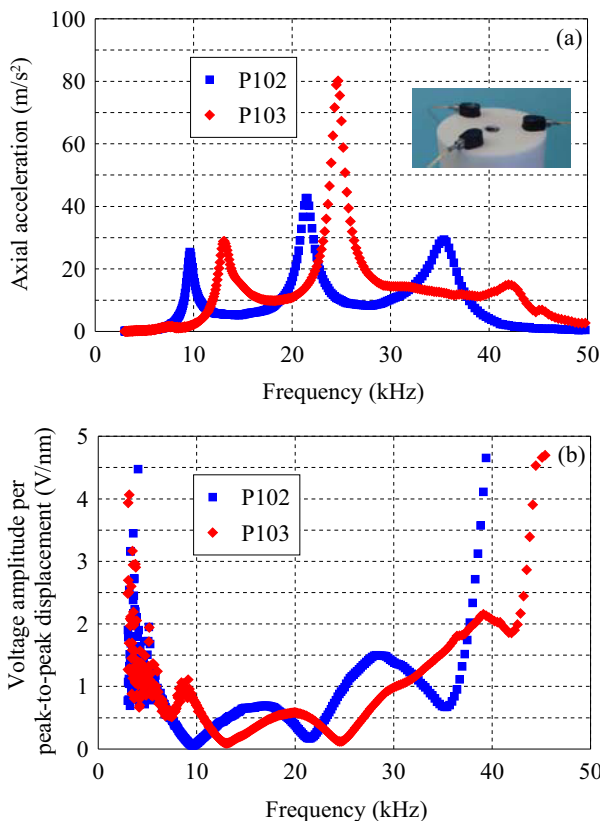


FIGURE 5. (a) Axial Acceleration and (b) Voltage Amplitude Per Peak-to-Peak Displacement versus Frequency for Piezo-Shakers P102 and P103 with $V_{pk} = 0.8$ V.

are needed at 30 kHz for shakers P102 and P103, respectively. However, application of Figure 5(b) for relatively large voltages and stresses is questionable due to nonlinearities of the piezoelectric material. In fact, elastic properties of lead zirconate titanate (PZT) ceramics can be distinctly nonlinear when compressive stresses exceed 20 MPa [14]. Nonetheless, the values from Fig. 5 should be on the same order of magnitude as those obtained for much higher voltages.

Impedance tests were also performed for model validation. A commercial impedance analyzer was used to measure the electrical impedance of each shaker through use of a constant voltage amplitude of 0.8 V, which is the

Now that a solution for the model equations is at hand, the model needs to be tested with experimental data. Therefore, three uniaxial accelerometers (approx. 0.5 grams each) were attached to the tables of shakers P102 and P103 with wax, as seen in the small insert of Figure 5(a). Each shaker was then driven with a voltage $V(t)$ of varying frequency but with a fairly constant source amplitude of 0.8 V from a dynamic signal analyzer. Voltage data were acquired for all three accelerometers. However, for simplicity, only two of the voltage signals were processed with 8th-order fits of the respective calibrated sensitivities as functions of frequency. Finally, the resulting accelerations were averaged per shaker.

Figure 5(a) shows the resulting (averaged) acceleration frequency responses, and Fig. 5(b) displays voltage per peak-to-peak displacement. The accelerations from Fig. 5(a) were used to calculate the displacements needed for Fig. 5(b). Note that Fig. 5(b) is somewhat like the inverse of the frequency response, since the resonances in Fig. 5(a) correspond closely to the minima in Fig. 5(b) and the minima in Fig. 5(a) are similar in frequency to the maxima in Fig. 5(b).

Figure 5(b) is useful because it reveals the voltages necessary for a desired peak-to-peak displacement. For example, for the fringe-disappearance method for accelerometer calibrations [12, 13] in which an approximately 121 nm displacement range is needed, Figure 5(b) reveals that voltage amplitudes of about 180 V and 120 V

same as that used for the accelerometer tests. The magnitude, Z , and phase, θ , versus frequency are seen for both shakers in Fig. 6, where the complex impedance \tilde{Z} is related to the voltage phasor \tilde{V} and the current phasor \tilde{I} by

$$\tilde{V} = \tilde{Z}\tilde{I} = Ze^{j\theta}\tilde{I} \quad (24)$$

and j is the imaginary unit.

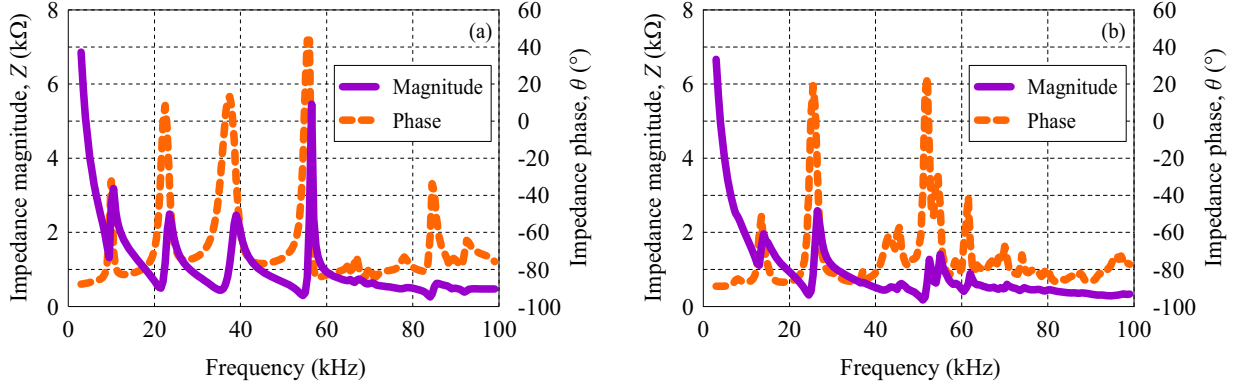


FIGURE 6. Measured Electrical Impedance for (a) Shaker P102 and (b) Shaker P103 with $V_{pk} = 0.8$ V.

MODEL VALIDATION

The model can now be tested through use of the experimental acceleration and impedance data. To this end, we create a basic electrical model to simulate electrical excitation of the shaker.

Figure 7(a) shows a RLC circuit with resistance R_s , inductance L_s , and capacitance C_s that is in series with the shaker. All capacitors have imperfections that create series resistance, and similarly, the leads to the piezoelectric ceramic disks add series inductance. Furthermore, electrical impedances are added to the system through use of voltmeters and other instrumentation that are partly accounted for in the model. A parallel capacitance C_p also aids to account for the self capacitance of the transducer.

Figure 7(b) shows the electrical excitation model in its phasor space, where Z_{piezo} is the complex impedance of the shaker resulting from the model for axial vibrations. In order to calculate Z_{piezo} as a function of frequency, we first calculate the shaker masses based on the densities in Table 1 and the known geometries. Then, we choose the remaining four system parameters (k_1 , k_2 , c_1 , and c_2) and solve the complete system of linear equations for the model. Equation (3) is then utilized to calculate the displacement currents I_u and I_l in the upper and lower piezo disks, respectively, and their sum is substituted into Eq. (24) to determine Z_{piezo} . Finally, the total complex impedance, Z_{total} , for the circuit in Fig. 7(b) is determined through use of standard circuit impedance rules [15] with the four chosen electrical parameters (R_s , L_s , C_s , and C_p).

Figure 8 shows the comparison of the magnitude and phase of Z_{total} for the model of shaker P102 with the experimental results from Fig. 6(a). Figure 8(a) reveals that the three frequencies at approximately 10 kHz, 21 kHz, and 35 kHz are fairly well matched by the model. The modes at these frequencies are basically those for coupled rigid bodies. Consequently, the chosen parameters listed in the caption of Fig. 8 are by no means optimal, but adequate for illustrative purposes. However, the fourth experimental resonance at about 45 kHz is not captured in the simulated impedance. One possible reason for this discrepancy is that the response at 45 kHz is not for an axial

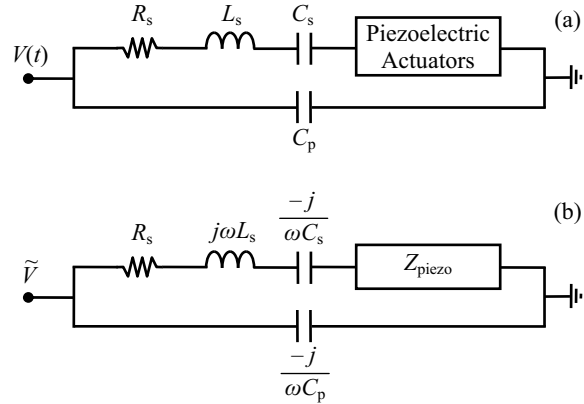


FIGURE 7. Schematic of Electrical Model for Shaker Excitation in (a) Real-Time and (b) Phasor Space.

mode, but rather for a lateral mode, of the piezoelectric ceramic actuators. The model, having been developed for only axial displacements, cannot capture lateral modes. On the other hand, the impedance analyzer captures the full impedance and is therefore influenced by axial, lateral, and other motions of the piezoelectric ceramic.

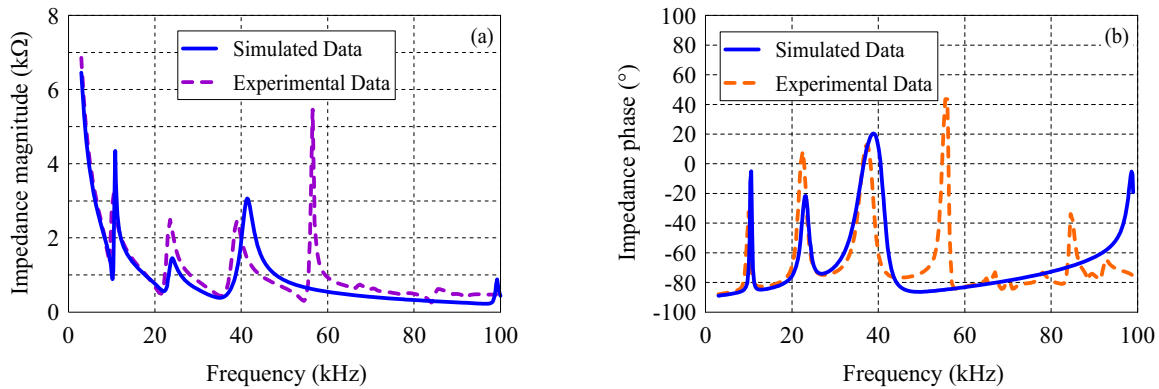


FIGURE 8. Simulated versus Experimental (a) Magnitude and (b) Phase for Shaker P102 with these Parameters: $k_1 = 2.6 \text{ N/nm}$, $k_2 = 4.2 \text{ N/nm}$, $c_1 = 1500 \text{ N}\cdot\text{s/m}$, $c_2 = 2500 \text{ N}\cdot\text{s/m}$, $R_s = 250 \text{ }\Omega$, $L_s = 0.6 \text{ mH}$, $C_s = 20 \text{ nF}$, and $C_p = 2.5 \text{ nF}$.

Nonetheless, the model does have four modes that are visible in Figure 8. While the first three modes for the model correspond to typical modes of coupled rigid bodies, the fourth mode at about 100 kHz corresponds mainly to an internal mode of the bonded piezoelectric disks. Figure 9 shows this mode shape for the model of shaker P102. The interface of the piezoelectric disks at $z = 0$ moves the most, while the two ends of the actuator do not move relatively as much. Consequently, the piezoelectric disks resonate together without a lot of interaction with the rigid masses. The experimental data in Fig. 8 possibly supports the existence of this mode, albeit at a lower frequency near 85 kHz.

Another check of the model is to simulate the acceleration of the shaker table and compare it to the experimental data in Fig. 5. For this comparison, the system parameters remained the same except for the series resistance R_s , which was decreased from $250 \text{ }\Omega$ to $25 \text{ }\Omega$. The former resistance was determined after data processing to be caused primarily by the impedance analyzer, which inadvertently adds a large resistance if the electrical contacts are not suitable. The dynamic signal analyzer was used instead of the impedance analyzer for the accelerometer tests, and since the source impedance of the analyzer is specified to be less than $5 \text{ }\Omega$, no other impedance sources were added to the model of Fig. 7.

Figure 10 shows the resulting simulated voltage per displacement and axial acceleration for shaker P102. With increasing frequency, the modeled damping appears to be too small, then acceptable, and then too large, compared to the experimental data at the resonances. This shows that damping should be better modeled, but with only two damping parameters, the fitting of parameters was limited. Consequently, perhaps another significant damping source was neglected that should be included in a future attempt at modeling piezoshakers, e.g., damping within the piezoelectric ceramic.

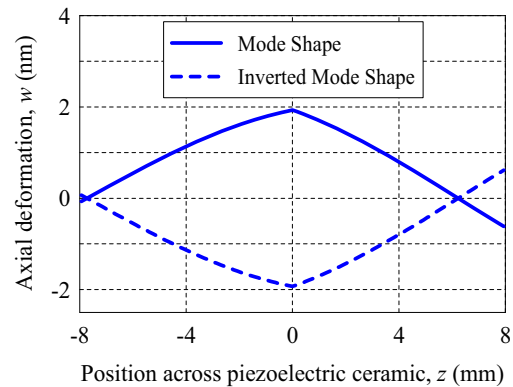


FIGURE 9. Piezoelectric Ceramic Mode Near 100 kHz for Simulated Excitation of Shaker P102.

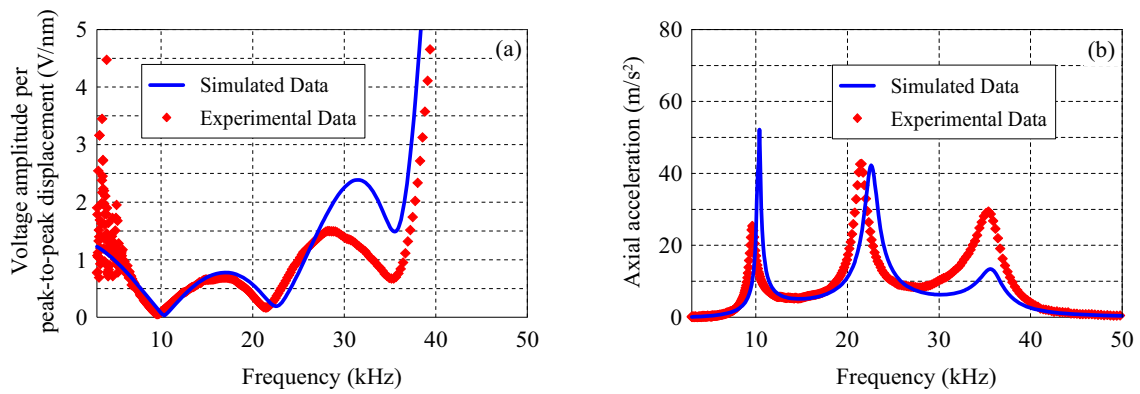


FIGURE 10. Simulated versus Experimental (a) Voltage Per Displacement and (b) Acceleration for Shaker P102 with $k_1 = 2.6$ N/mm, $k_2 = 4.2$ N/mm, $c_1 = 1500$ N•s/m, $c_2 = 2500$ N•s/m, $R_s = 25$ Ω , $L_s = 0.6$ mH, $C_s = 20$ nF, and $C_p = 2.5$ nF.

CONCLUSIONS

In this paper, we presented a model of piezoelectric shakers and compared its predictions to experimental data. The piezoelectric actuator was modeled as a compliant element governed by coupled state equations, and the other shaker parts were modeled as either rigid bodies (alumina or tungsten carbide cylinders) or simple compliant elements (butyl rubber). Twenty-four linear algebraic equations governing the physics of the shaker were created and solved. For any set of system parameters (two stiffness and two damping coefficients), an electrical impedance can be generated from the solution for use with model validation.

By considering the excited shaker as a system with a modified impedance due to additional electrical elements, we demonstrated that the results from the model agree fairly well with those from impedance and acceleration experiments. However, some discrepancies in resonant frequencies and damping exist. Therefore, future improvements include the addition of system nonlinearities, piezoelectric ceramic radial displacements, cross-axial and rotational motion of rigid bodies, piezoelectric ceramic damping, transduction irreversibility, and frequency-dependent parameters. These improvements to the model, coupled with further model validation, should illustrate how modeling of piezoelectric shakers can be used as a design tool to maximize their performance for the high-frequency calibration of accelerometers before shaker assembly begins.

REFERENCES

1. E. Jones, W. B. Yelon, and S. Edelman, "Piezoelectric Shakers for Wide-Frequency Calibration of Vibration Pickups", *The Journal of the Acoustical Society of America* **45**(6), 1556-1559 (1969).
2. B. Payne, K. Harper, and G. W. Vogl, "Piezoelectric Shaker Development for High Frequency Calibration of Accelerometers", to be published (2010).
3. G. P. Ripper, R. S. Dias, and G. A. Garcia, "Primary Accelerometer Calibration Problems due to Vibration Exciters", *ELSEVIER, Measurement* **42**, 1363-1369 (2009).
4. J. Xue and T. He, "The Application of Bessel Function Methods on High Frequency Vibration Calibration", *SPIE* **5503**, 423-430 (2004).
5. W. D. Callister, Jr., *Materials Science and Engineering: An Introduction*, 4th Ed., New York: John Wiley & Sons, Inc., 1997, pp. 775-778.
6. K. Liu, X. P. Li, M. Rahman, and X. D. Liu, "CBN Tool Wear in Ductile Cutting of Tungsten Carbide" in *14th International Conference on Wear of Materials*, edited by P. J. Blau and R. G. Bayer, ELSEVIER B.V., 2003, pp. 1344-1351.
7. American Piezo Ceramics Inc., *Piezoelectric Ceramics: Principles and Applications*, Mackeyville, Pennsylvania: APC International Ltd., 2009, p. 30.
8. S.-F. Ling and Y. Xie, "Detecting Mechanical Impedance of Structures using the Sensing Capability of a Piezoceramic Inertial Actuator, *Sensors and Actuators A* **93**, 243-249 (2001).
9. D. Damjanovic, M. Demartin, H. Shulman, and N. Setter, "Instabilities in Piezoelectric Properties of Ceramic Sensors and Actuators under Extreme Conditions" in *The 8th International Conference on Solid-State Sensors and Actuators and Eurosensors IX*, Vol. 2, 1995, pp. 218-221.
10. T. S. Edwards, "Using Passively Shunted Electromechanical Transducers to Control the Boundary Impedance of Dynamic Test Fixtures", *Journal of Sound and Vibration* **323**, 33-50 (2009).

11. R. R. Ramos, J. A. Otero, and R. Pérez-Alvarez, "Wave Propagation in a Piezoelectric Layer", *Journal of Applied Physics* **81**(11), 7242-7247 (1997).
12. ISO 16063-11, *Methods for the calibration of vibration and shock transducers — Part 11: Primary vibration calibration by laser interferometry*, Geneva: International Organization for Standardization, 1999.
13. D. C. Robinson, M. R. Serbyn, and B. F. Payne, "A Description of NBS Calibration Services in Mechanical Vibration and Shock", NBS Technical Note, 1232 (1987).
14. D. A. Hall, "Nonlinearity in Piezoelectric Ceramics", *Journal of Materials Science* **36**, 4575-4601 (2001).
15. L. Weinberg, *Network Analysis and Synthesis*, New York: Robert E. Krieger Publishing Company, 1975.